Hindawi Publishing Corporation
Journal of Wind Energy
Volume 2015, Article ID 895974, 12 pages
http://dx.doi.org/10.1155/2015/895974

Research Article

Separated Pitch Control at Tip: Innovative Blade Design Explorations for Large MW Wind Turbine Blades

Ranjeet Agarwala[1,2] and Paul I. Ro[2]

[1]*Department of Technology Systems, East Carolina University, Greenville, NC 27545, USA*
[2]*Department of Mechanical and Aerospace Engineering, North Carolina State University, Raleigh, NC 27695, USA*

Correspondence should be addressed to Ranjeet Agarwala; agarwalar@ecu.edu

Received 26 August 2014; Accepted 22 January 2015

Academic Editor: Jianzhong Zhang

This paper focuses on the deployment and evaluation of a separated pitch control at blade tip (SePCaT) control strategy for large megawatt (MW) wind turbine blade and explorations of innovative blade designs as a result of such deployment. SePCaT configurations varied from five to thirty percent of the blade length in 5 percentage increments (SePCaT5, SePCaT10, SePCaT15, SePCaT20, SePCaT25, and SePCaT30) are evaluated by comparing them to aerodynamical responses of the traditional blade. For low, moderate, high, and extreme wind speed variations treated as 10, 20, 30, and 40 percent of reference wind speeds, rotor power abatement in region 3 of the wind speed power curve is realized by feathering full length blade by 6, 9, 12, and 14 degrees, respectively. Feathering SePCaT30, SePCaT25, SePCaT20, and SePCaT15 by 14, 16, 26, and 30 degrees, respectively, achieves the same power abatement results when compared to traditional blade at low wind speeds. Feathering SePCaT30, SePCaT25, and SePCaT20 by 18, 26, and 30 degrees on the other hand has the same effect at high wind speeds. SePCaT30 feathered to 26 and 30 degrees has the same abatement effects when compared to traditional blade at high and extreme wind speeds.

1. Introduction

The growth of large wind turbines manifests many design challenges as rotor sizes and tower heights scale to continue to accommodate larger land based and offshore wind turbine power capacities. At high wind speeds, wind turbines are primarily controlled by varying the blade pitch angle at the rotor hub. Abatement of load is accomplished by pitching the blades to either feather or stall with the former being more desirable. Mechanisms for full length pitching are also large, complex, and expensive requiring higher manufacturing and maintenance costs. Therefore, as wind turbines continue to grow in size and achieve power ratings to the order of 10 MW or higher, independent or collective full length pitch control becomes increasingly cumbersome. Many researchers have proposed alternate control strategies for wind turbines. Some of these include telescopic blades, trailing edge-flaps, transitional tabs, plasma actuation, flow detectors, and active flaps to name a few [1–8]. Daynes and Weaver [9, 10] conducted tests on a NACA63-418 blade section equipped with a 20 percent chord length trailing edge-flap controller and observed that the lift coefficient changed by a value of 1.0 when the flap angle was varied from −10 to 10 degrees. Houtzager et al. [11] conceptualized a smart wind turbine rotor where blades were installed with transitional tabs and trailing edge-flaps, thereby reducing load variance by 42 percent. Versailles et al. [12] assessed the effectiveness of plasma actuation to control lift force of a wind turbine blade and observed a lift mitigation of 30 to 50 percent. Barlas and van Kuik [6] and Barlas et al. [5] incorporated active flaps for load control of the 5 MW NREL/upwind reference wind turbine blade reducing load by 27 percent. Bai et al. [7] deployed flow deflectors enhancing lift by 24 percent and causing the stall to be delayed by 2 degrees. Lee and Su [8] investigated an airfoil equipped with a 25 percent trailing edge-flap controller in addition to a Gurney flap and reported that the flap controller at stall caused the lift coefficient to be enhanced from 1.1 for the baseline flap angle to a value of 1.55 for a flap angle of 18 degrees. Bottalla et al. [13] investigated the effect of trailing edge-flap and tab and

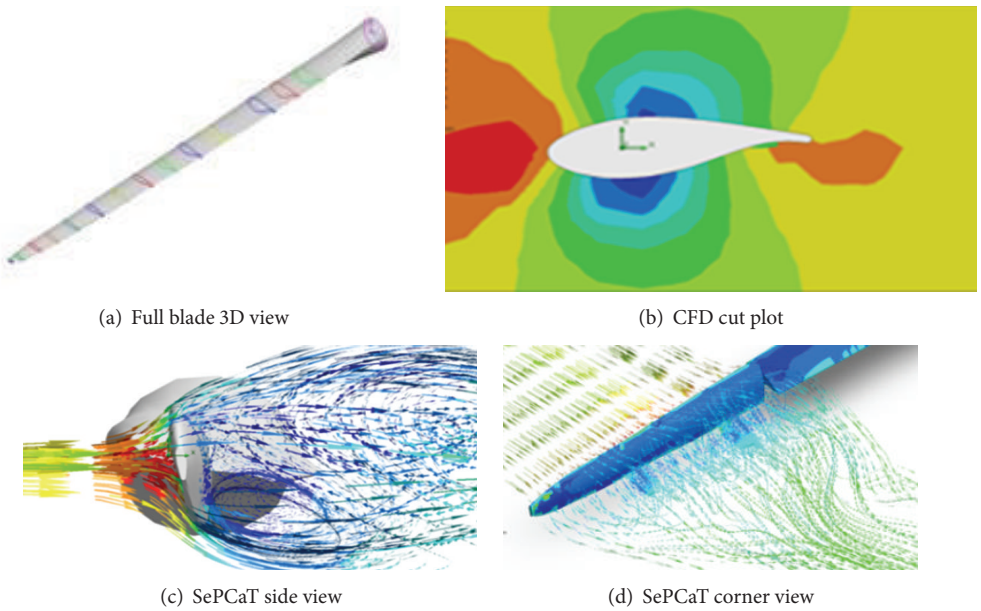

(a) Full blade 3D view (b) CFD cut plot

(c) SePCaT side view (d) SePCaT corner view

Figure 1: Traditional SePCaT wind turbine configurations. The 3D CAD model along with CFD environment for the traditional blade and SePCaT.

reported that the lift coefficient around stall was enhanced from 0.6 at a flap angle of 30 degrees counterclockwise to 1.7 at a flap angle of 30 degrees clockwise. On the other hand, the tab controller which measured one-fourth of flap enabled enhancement of the lift coefficient at stall from 1.2 at 30 degrees counterclockwise to 1.7 at 30 degrees clockwise. Heinz et al. [14] researched an adaptive trailing edge-flap controller equipped with piezoelectric actuators enabling load mitigation of up to 76 percent. Markou et al. [15] proposed load reductions of up to 73 percent by using deformable trailing edge-flap controllers on a 5 MW wind turbine. Andersen et al. [16] used a 6.3 m long trailing edge-flap controller to mitigate the loads by 25 percent on a 5 MW wind turbine blade. Johnson et al. [17] utilized microtabs of the order of 1.5 percent of chord length in enhancing and mitigating the lift by 37 and 40 percent for a 5-degree angle of attack. Wilson et al. [18] investigated trailing edge-flaps for controlling and mitigating aerodynamic loads by 20–30 percent enabling energy optimization. All of these wind turbine control surface designs, researches, and analyses were based on 2D analysis. 2D analysis does not take into account the structural twist of the blade, the effect of varying airfoil sectional geometries, and the type of airfoil which have profound influence on aerodynamic loads and impact wind turbine power generation. Agarwala and Ro [2] focused on 3D aerodynamic analysis and control of a wind turbine blade via 3D control surface design and deployment of trailing edge mid- and end-flaps. Partial spanwise trailing-edge 3D control surfaces were modeled, simulated, and analyzed at various control angles. Results depicted the onset of stall around 22 degrees and a larger lift gain versus 10–15 degrees for standard 2D airfoils. Midflap controller enhanced lift by a factor 2 and mitigated moment by a factor of around 7 while end-flap controller enhanced lift by a factor of around 1.024 and mitigated moment by a factor of around 2. Although telescopic blades, trailing edge-flaps, transitional tabs, plasma actuation, flow detectors, and so forth alleviate some of these problems, nevertheless they lead to manufacturing, maintenance, deployment, and actuation complexities.

Some researchers have proposed alternate methods and ideas similar to SePCaT and its associated strategies. Imraan et al. [1] conceptualized telescopic wind turbine blades having chord ratios of 0.6 and studied the influence of blade extension on blade loads. Mechanism proposed by them allowed linear actuation of the blade length for load adaptation. Their methods although novel present complexities and increased manufacturing costs. Peter et al. [3] in their patent proposed a partial pitch rotor blade 35 meters in diameter comprising an inner and outer blade portion with the pitch mechanism pitching the outer blade with respect to inner blade. Nothing further with regard to optimum lengths and pitch angle configurations of both inner and outer blade segment and comparison to that of traditional control methods through detailed CFD analysis has been proposed.

Investigation and evaluation of a novel separated pitch control at blade tip (SePCaT) control strategy and comparison to traditional pitch control for a large MW wind turbine are conducted to gage the effectiveness of this novel deployment. The paper is structured as follows. Theory is discussed in Section 2. Aerodynamics and CFD model are discussed in Section 3. Numerical results and analysis are discussed in Section 4. Exploration of innovative blade design is covered in Section 5 and conclusions are discussed in Section 6.

2. Theory

The blade is first modeled as a standalone CAD model as shown in Figure 1(a) using SolidWorks from Dassault

Table 1: Parameters for 2D aerodynamic equations.

A	Pitch of attack for main blade	rad
$\mathrm{PB}_{\mathrm{CA}}$	Control angle for partial blade	rad
U	Wind velocity	ms^{-1}
h	Plunge	m
d	Airfoil chord length for main blade	m
b	Airfoil chord half-length for main blade	m
l	Length of the blade for main blade	m
a	Fraction of chord distance between pitch axis (PA) and midchord (MC)	—
e	Fraction of chord distance between PA and aerodynamic center (AC)	—
d_{PB}	Airfoil chord length for SePCaT	m
b_{PB}	Airfoil chord half-length for SePCaT	m
l_{PB}	Length of the blade for SepCAT	m
a_{PB}	Fraction of chord distance between (PA) and MC for SePCaT	—
e_{PB}	Fraction of chord distance between PA and AC for SePCaT	—
ρ	Density of air	kgm^{-3}
C_{TH}	Theodorsen's function	—
CM_A	Moment coefficient per angle of attack	—
CL_A	Lift coefficient per angle of attack	—
$\mathrm{CMPB}_{\mathrm{CA}}$	Moment coefficient per partial blade control angle	—
$\mathrm{CLPB}_{\mathrm{CA}}$	Lift coefficient per partial blade control angle	—

systems. Various airfoil shapes at different locations of the wind turbine blade are based on geometrical properties and coordinates of the model 5 MW NREL wind turbine blade [19]. Airfoil curves at various cross sections are generated using Cartesian coordinate systems. Airfoils at each section are scaled and rotated by their chord lengths and values of angular twists. Various cross sections are connected together using inbuilt CAD modeling interpolation routines [2].

3D control surfaces are deployed as separated sections of partial blade length at the blade tip as depicted in Figures 1(c) and 1(d). The 2D quasisteady aerodynamic equations of an airfoil and the SePCaT are based on parameters as given in Table 1. For a small section of blade as per Figure 2, the lift force and moment [19–21] are given in (1). The lift force at the aerodynamic center of any blade section is caused due to the pressure difference between the upper and lower surface of the airfoil when the air flows past that airfoil section. The pressure difference is caused due to the geometry; in particular, the camber of the airfoil produces varying velocities at the top and bottom surface of the airfoil. The pressure difference when multiplied by the area of a section of the blade of length produces the lift force of dL.

The lift coefficient is nondimensional term that captures the geometry of the airfoil impacted by lift forces. Similarly, the aerodynamic moment is computed by multiplying the vertical forces with the chord length. The moment coefficient

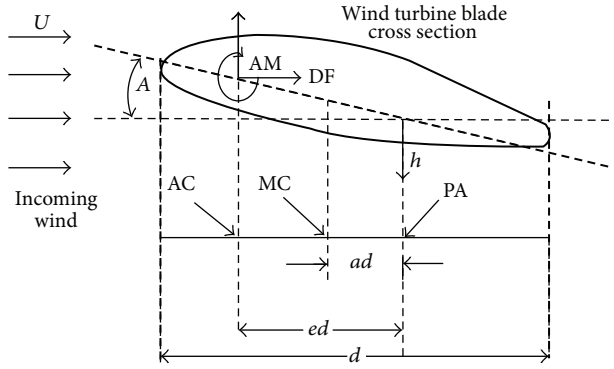

Figure 2: Cross-section of a wind turbine blade. 2D quasisteady aerodynamic equations of an airfoil and the SePCaT are based on parameters as depicted here.

is a nondimensional term that captures the geometry of the airfoil impacted by aerodynamic moment:

$$dL = \frac{1}{2}\rho U^2 d\mathrm{CL}_A dl + \frac{1}{2}\rho U^2 d_{\mathrm{PB}} \mathrm{CL}_{\mathrm{PB}_{\mathrm{CA}}} dl_{\mathrm{PB}},$$
$$dM = \frac{1}{2}\rho U^2 d^2 \mathrm{CM}_A dl + \frac{1}{2}\rho U^2 {d_{\mathrm{PB}}}^2 \mathrm{CM}_{\mathrm{PB}_{\mathrm{CA}}} dl_{\mathrm{PB}}. \quad (1)$$

The total combined lift and moment for the main blade and SePCaT are obtained by integrating the lift and moment values for the entire blade length exposed to wind and are given in the following equation:

$$L = \frac{1}{2}\rho U^2 d\mathrm{CL}_A \int_0^l dl + \frac{1}{2}\rho U^2 d_{\mathrm{PB}} \mathrm{CL}_{\mathrm{PB}_{\mathrm{CA}}} \int_0^{l_{\mathrm{PB}}} dl_{\mathrm{PB}},$$
$$M = \frac{1}{2}\rho U^2 d^2 \mathrm{CM}_A \int_0^l dl + \frac{1}{2}\rho U^2 {d_{\mathrm{PB}}}^2 \mathrm{CM}_{\mathrm{PB}_{\mathrm{CA}}} \int_0^{l_{\mathrm{PB}}} dl_{\mathrm{PB}}. \quad (2)$$

The unsteady airfoil moment and lift are dependent on the first and second derivatives of the airfoil plunge, pitch angle of the overall blade and its first and second derivatives, control angle of SePCaT and its first and second derivatives, velocity of air, density of air, and time as shown in (3). Figure 2 depicts the setup of the main blade and the SePCaT control surface along with airfoil cross section. Figure 2 and lift and moment equations are based on the literature and previous research [21–24]:

$$L = L\left(\dot{h}, \ddot{h}, A, \dot{A}, \ddot{A}, \mathrm{PB}_{\mathrm{CA}}, \dot{\mathrm{P}}\mathrm{B}_{\mathrm{CA}}, \ddot{\mathrm{P}}\mathrm{B}_{\mathrm{CA}}, U, \rho, \mathrm{time}\right),$$
$$M = M\left(\dot{h}, \ddot{h}, A, \dot{A}, \ddot{A}, \mathrm{PB}_{\mathrm{CA}}, \dot{\mathrm{P}}\mathrm{B}_{\mathrm{CA}}, \ddot{\mathrm{P}}\mathrm{B}_{\mathrm{CA}}, U, \rho, \mathrm{time}\right). \quad (3)$$

The total airfoil lift and moment are a combination of steady state lift due to circulatory motion based on blade pitching, lift due to noncirculatory motion caused by blade pitching

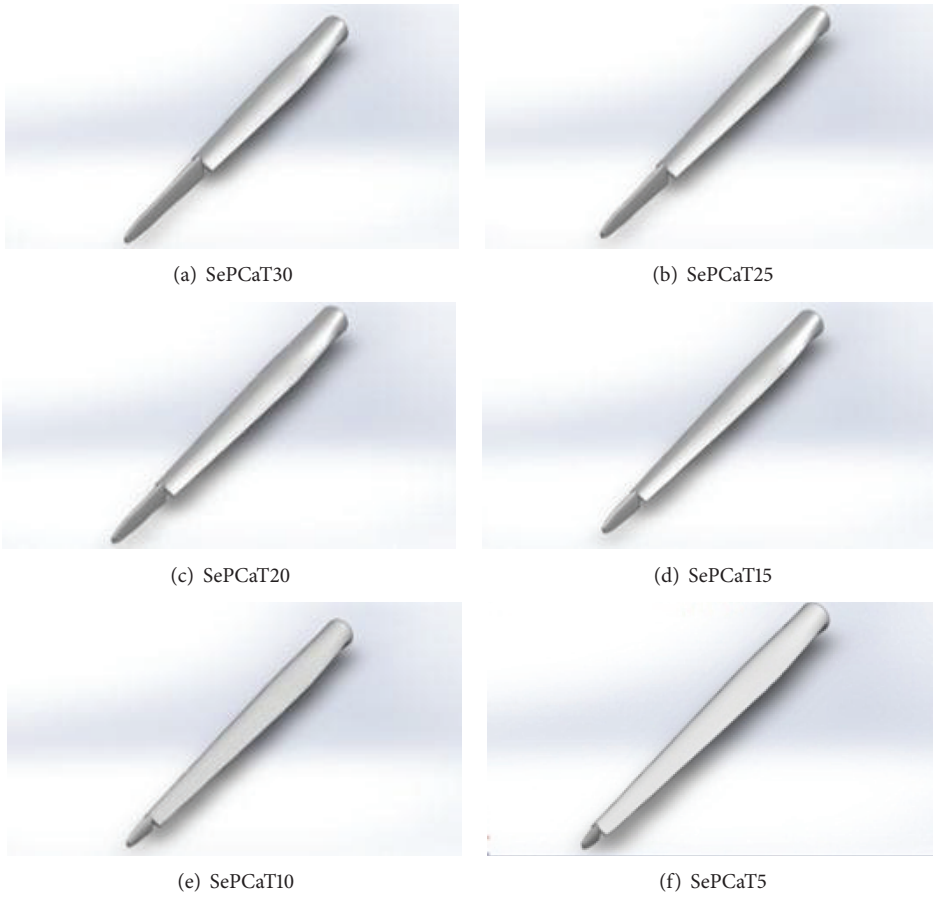

(a) SePCaT30 (b) SePCaT25

(c) SePCaT20 (d) SePCaT15

(e) SePCaT10 (f) SePCaT5

Figure 3: SePCaT setups. The length of SePCaT is varied from five to thirty percent of the blade length in 5-degree increments.

and plunging, and lift change due to the pitch, plunge, and angular position of the control surface as shown in

$$\begin{aligned} L &= L_{\text{steady state}} + L_{\text{circulatory motion}} \\ &\quad + L_{\text{noncirculatory motion}} + L_{\text{control surface}}, \\ M &= M_{\text{steady state}} + M_{\text{circulatory motion}} \\ &\quad + M_{\text{noncirculatory motion}} + M_{\text{control surface}}. \end{aligned} \tag{4}$$

The unsteady airfoil lift and moment are based on the unsteady aerodynamic theory [21–24] as shown in (5). The parameters are provided in Table 1:

$$\begin{aligned} L &= \pi\rho b^2 \left(\ddot{h} + U\dot{A} - ba\ddot{A}\right) \\ &\quad + 2\pi\rho U C_{\text{TH}} b \left[\dot{h} + UA + \left(\frac{1}{2} - a\right) b\dot{A}\right], \\ M &= -\pi\rho b^3 \left[-a\ddot{h} + \left(\frac{1}{2} - a\right) U\dot{A} + \left(\frac{1}{8} - a^2\right) b\ddot{A}\right] \\ &\quad + 2\pi\rho U C_{\text{TH}} b^2 \left[\left(\frac{1}{2} + a\right)\left(\dot{h} + UA + \left(\frac{1}{2} - a\right)\dot{A}\right)\right]. \end{aligned} \tag{5}$$

Detailed derivation of (5) is cited in many previous literatures and researches. Readers are encouraged to refer to the cited literature [21–24] for further reading.

3. Aerodynamic and CFD Model

The entire blade along with SePCaT is designed using the 5 MW National Renewable Energy Laboratory (NREL) [19] turbine specifications in three dimensions (3D) and analyzed using 3D computational fluid dynamics (CFD) routines. The software used for the analysis of both CAD and CFD was SolidWorks from Dassault systems. The CFD settings are programmed to emulate region three of the wind turbine power curve where abatement of excessive rotor power is warranted due to high wind speeds to maintain rated power.

3D control surfaces are deployed as separated sections of partial blade length at the tip as shown in Figure 3(a) through Figure 3(f). The length of SePCaT is varied from five to thirty percent of the blade length in 5-degree increments (SePCaT5, SePCaT10, SePCaT15, SePCaT20, SePCaT25, and SePCaT30).

Lift and moment equations with SePCaT deployed as shown in Figure 3 are depicted in (6). The parameters for each term of the equation are provided in Table 1. The second

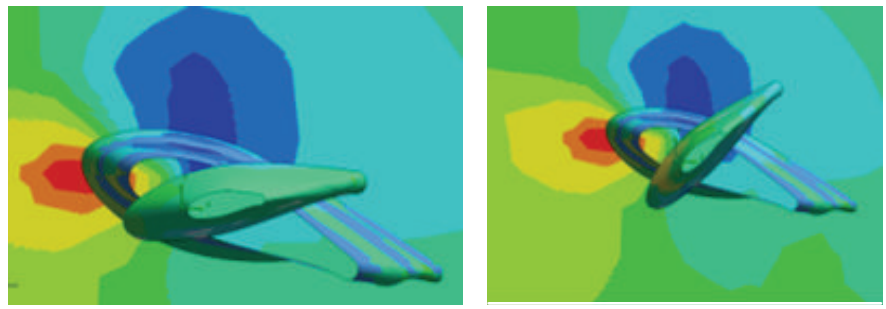

Figure 4: Traditional blade with SePCaT-pitch to feather.

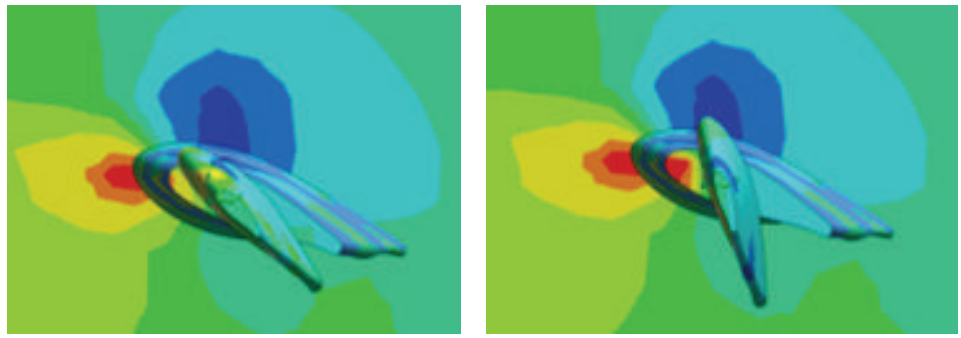

Figure 5: Traditional blade with SePCaT-pitch to feather.

term on the right hand side of the equations represents a contribution due to SePCaT, as indicated in the equations:

$$L = \rho U^2 b \mathrm{CL}_A \left[A + \frac{\dot{h}}{U} + \left(\frac{1}{2} - a\right) b \frac{\dot{A}}{U} \right] + \underbrace{\rho U^2 b_{\mathrm{PB}} \mathrm{CL}_{\mathrm{PBCA}} \left[\mathrm{PB}_{\mathrm{CA}} + \frac{\dot{h}}{U} + \left(\frac{1}{2} - a_{\mathrm{PB}}\right) b_{\mathrm{PB}} \frac{\dot{\mathrm{PB}}_{\mathrm{CA}}}{U} \right]}_{\mathrm{SePCaT}},$$

$$M = \rho U^2 b^2 \mathrm{CM}_A \left[A + \frac{\dot{h}}{U} + \left(\frac{1}{2} - a\right) b \frac{\dot{A}}{U} \right] + \underbrace{\rho U^2 {b_{\mathrm{PB}}}^2 \mathrm{CM}_{\mathrm{PBCA}} \left[\mathrm{PB}_{\mathrm{CA}} + \frac{\dot{h}}{U} + \left(\frac{1}{2} - a_{\mathrm{PB}}\right) b_{\mathrm{PB}} \frac{\dot{\mathrm{PB}}_{\mathrm{CA}}}{U} \right]}_{\mathrm{SePCaT}}. \quad (6)$$

Lift and moment equations for exclusive SePCaT actuations reduce to

$$L_S = \rho U^2 b \mathrm{CL}_A \left[A + \frac{\dot{h}}{U} \right] + \rho U^2 b_{\mathrm{PB}} \mathrm{CL}_{\mathrm{PBCA}} \cdot \left[\mathrm{PB}_{\mathrm{CA}} + \frac{\dot{h}}{U} + \left(\frac{1}{2} - a_{\mathrm{PB}}\right) b_{\mathrm{PB}} \frac{\dot{\mathrm{PB}}_{\mathrm{CA}}}{U} \right],$$

$$M_S = \rho U^2 b^2 \mathrm{CM}_A \left[A + \frac{\dot{h}}{U} \right] + \rho U^2 {b_{\mathrm{PB}}}^2 \mathrm{CM}_{\mathrm{PBCA}} \cdot \left[\mathrm{PB}_{\mathrm{CA}} + \frac{\dot{h}}{U} + \left(\frac{1}{2} - a_{\mathrm{PB}}\right) b_{\mathrm{PB}} \frac{\dot{\mathrm{PB}}_{\mathrm{CA}}}{U} \right]. \quad (7)$$

Equations (5) have been modified to include SePCaT and take the form of (6) through (7). The main blade with SePCaT was first pitched to feather (P-F) by varying the SePCaT angle in the counterclockwise direction as depicted in Figure 4. The influence of SePCaT P-F on aerodynamic load adaptation is evaluated by initially varying the SePCaT angle broadly followed by precise variations in the counterclockwise direction.

The main blade with SePCaT was then pitched to stall (P-S) by varying the SePCaT angle broadly followed by precise variations in the counterclockwise direction as depicted in Figure 5.

SePCaT configurations are evaluated by comparing them to traditional blade. The blade was first subject to traditional feathering by varying the pitch angle in the counterclockwise direction by one-degree increments as depicted in Figure 6.

The blade was then pitched to stall by varying the pitch angle in the clockwise direction as depicted in Figure 7. The influence of pitch to stall control on aerodynamic load adaptation is evaluated by varying the pitch angle precisely in one-degree increment in the clockwise direction.

The CFD settings are programmed to emulate region three of the wind turbine power curve where abatement of excessive rotor power is warranted due to high wind speeds to maintain rated power. Table 2 provides the CFD settings

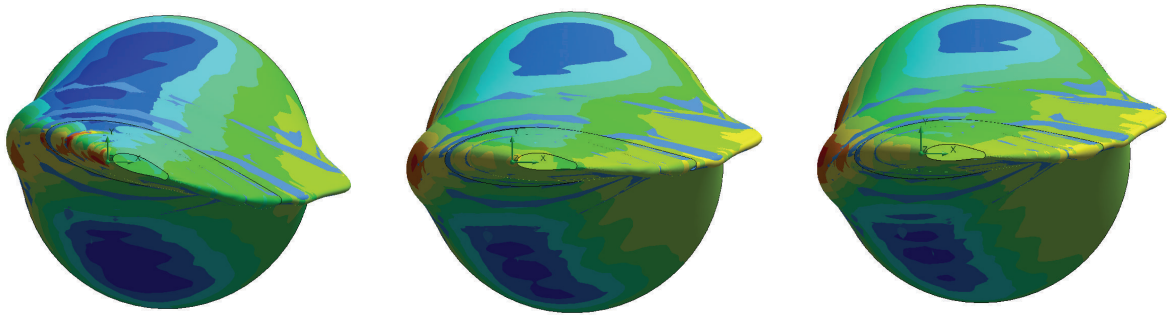

Figure 6: Traditional blade with SePCaT-pitch to feather.

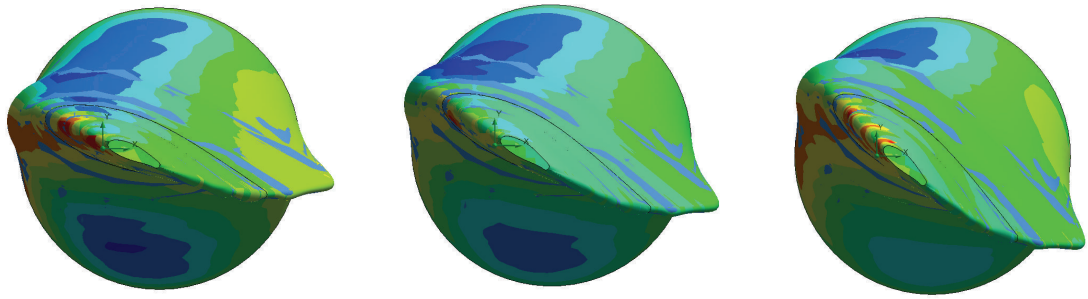

Figure 7: Traditional blade with SePCaT-pitch to stall.

Table 2: CFD settings.

Type of analysis	Laminar
X domain size	20 m
Y domain size	12 m
Z domain size	70 m
Type of mesh	Structured Cartesian (cuboid)
Total cells	502464
Total fluid cells	488670
Total solid cells	5657
Total partial cells	8137
Volume of cells	0.03 m^3

and environment. The numerical results are enumerated in Section 4.

4. Numerical Results and Analysis

SePCaT configurations varied from five to thirty percent of the blade length in 5 percentage increments (SePCaT5, SePCaT10, SePCaT15, SePCaT20, SePCaT25, and SePCaT30) are evaluated by comparing them to traditional blade. The computational domain was set at −10 m to 10 m along x-axis (direction of airflow), −6 m to 6 m along y-axis, and −5 m to 65 m along z-axis. The CFD responses of the traditional blade and its comparisons to blade with SePCaT are depicted in Figure 8.

Traditional P-F rotations of 7 degrees produce lift factor of 0.7. Lift factor reduction of 0.6 is achieved for P-F rotations of SePCaT25 by 26 and SePCaT30 by 20 degrees with traditional control producing the same lift factor at 9-degree P-F rotation. Lift factor of 0.5 is observed for P-F rotations of SePCaT25 by 36 and SePCaT30 by 24 degrees. Traditional P-F rotations on the other hand produce lift factor of 0.5 for 11-degree P-F rotations. Although SePCaT30 is capable of achieving lift factors of 0.3, 0.2, and 0.1, lift reduction of 0.4 and 0.3 can only be produced by SePCaT30 for P-F rotations of 28 and 36 degrees, respectively, in region void of lift degradation. Lift factors of 0.4, 0.3, 0.2, and 0.1 can be achieved by traditional P-F rotations of 13, 15, 17, and 18 degrees, respectively. It is observed from Figure 9 that 20-degree P-S rotations for all SePCaTs produce negligible lift reduction. Lift factors of 0.9 are observed for P-S rotations of SePCaT25 by 26 and of SePCaT30 by 24 degrees. Although SePCaT25 and SePCaT30 are capable of achieving lift factors of 0.8 and 0.7 at P-S rotations of 50 and 60 degrees, these regions experience stall and lift degradation. It is observed that lift factor reduction for all SePCaTs and traditional control is more pronounced when pitched to feather than when pitched to stall.

Region 3 of the NREL 5 MW model [19] wind turbine control is based on pitching the blades to feather to shed the excessive rotor power produced in the event of increasing wind speeds. Figure 10 depicts the comparisons of SePCaT and traditional control with respect to power shedding capabilities in region 3 of the wind turbine at low and moderate wind speed increments and variations. Power abatement factors versus feather angles in response to increasing wind speed are obtained from NREL studies [19]. NREL power factor curve represents the power reduction required in

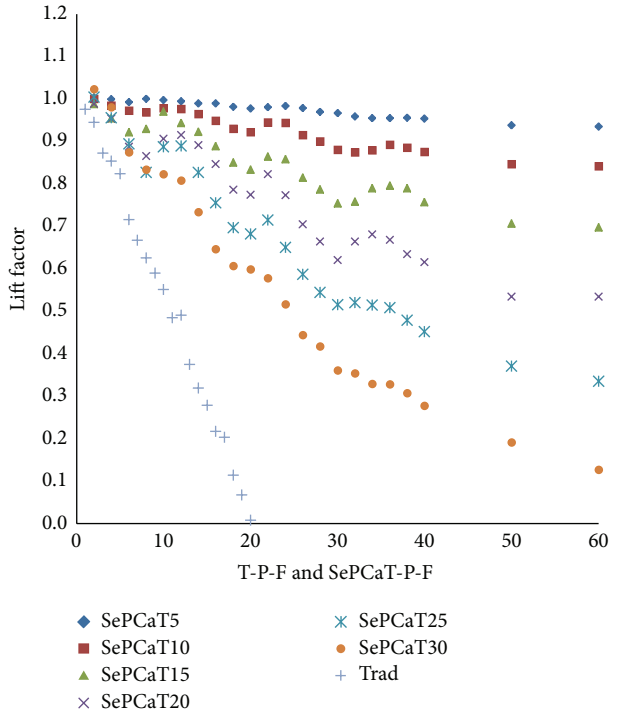

Figure 8: Pitch to feather SePCaTs versus traditional blade. Lift factor responses of the traditional blade and its comparisons to blade with SePCaT are depicted here.

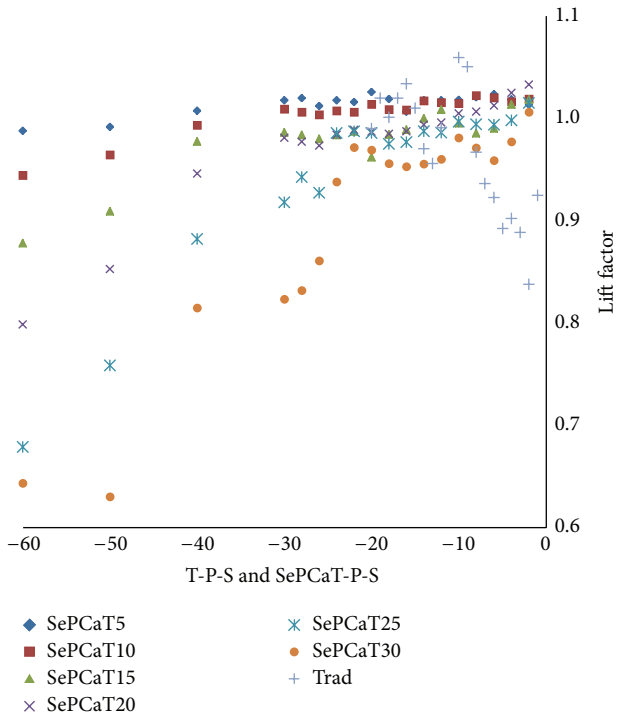

Figure 9: Pitch to stall SePCaTs versus traditional blade. Lift factor responses of the traditional blade and its comparisons to blade with SePCaT are depicted here.

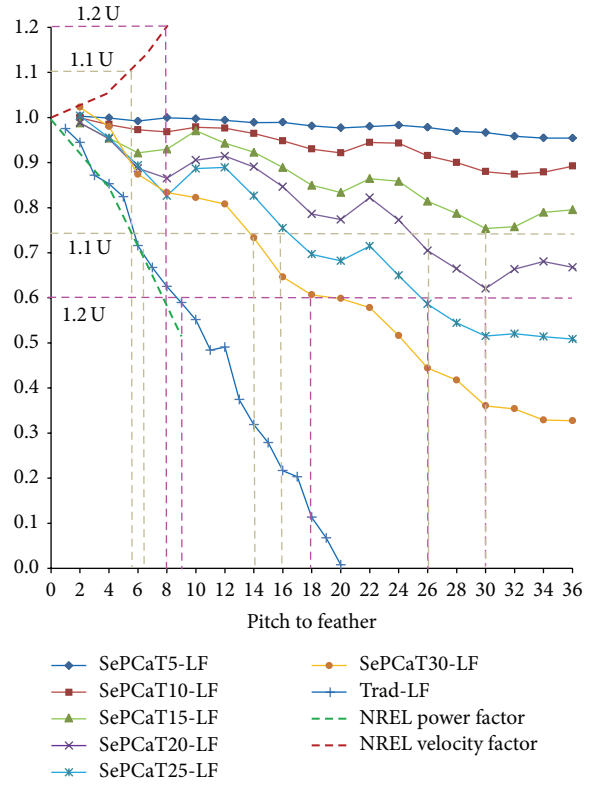

Figure 10: SePCaT versus traditional-rotor power abatement comparisons at low and moderate wind speed increments.

response to velocity increment factor depicted as NREL velocity factor curve.

The Appendix to this paper before References provides the traditional wind turbine specifications and CAD geometry of standard airfoil geometrical profiles and their locations along the blade length (stations) with regard to the traditional blade construction.

The data for power reduction versus pitch angle curve is obtained from NREL pitch angle setting recommendations to achieve set power factor reductions in response to velocity increments in region 3. As per the International Electrotechnical Commission (IEC), extreme wind speed (EWM) which is defined by 50-year and 1-year extreme wind recurrence probabilities is 40 and 30 percent higher than reference wind speed. Hence for the purposes of this study low, moderate, high, and extreme wind speeds increments were treated as being 10, 20, 30, and 40 percent more than the reference speed.

Figure 10 depicts power abatement requirement for low (1.1 U) and moderate (1.2 U) wind speed increments, respectively. According to NREL study, the model wind turbine has a rated power of 5 MW at the onset of region 3. This represents pitch angle settings of 0 degrees and a power factor of 1. As the wind speed increases by a factor of 1.1 U (10 percent), the rotor power increases to around 6.75 MW warranting its reduction to a factor of 0.74 approximately as shown by gray dotted line. To achieve this, the blade is feathered by around 6 degrees for traditional control. This is also achieved by

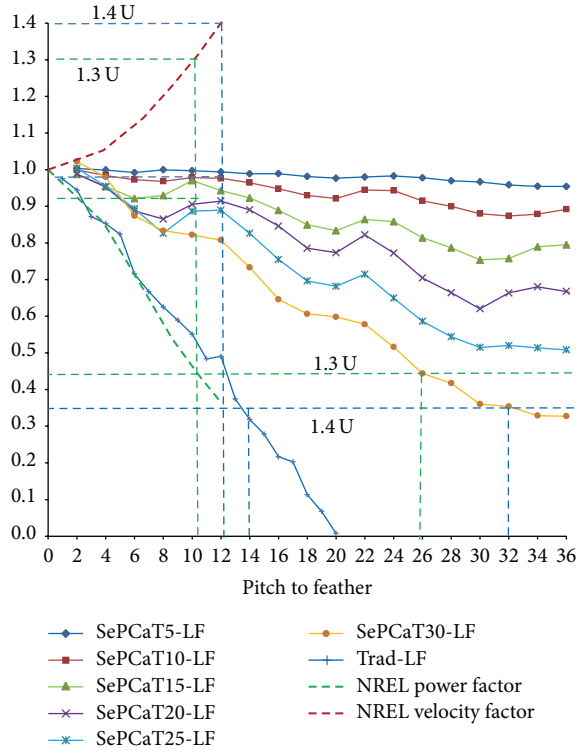

Figure 11: SePCaT versus traditional-rotor power abatement comparisons at high and extreme wind speed increments.

approximately feathering SePCaT30 by 14, SePCaT25 by 16 d, SePCaT20 by 26, and SePCaT15 by 30 degrees, respectively. If wind speed increases by a factor of 1.2 U (20 percent), the rotor power increases to around 8.33 MW warranting its reduction to a factor of 0.6 approximately as shown by magenta dotted line. To achieve this, the blade is feathered by around 9 degrees for traditional. This is also achieved by approximately feathering SePCaT30 by 18, SePCaT25 by 26, and SePCaT20 by 30 degrees, respectively.

Figure 11 depicts power abatement requirement for high (1.3 U) and extreme (1.4 U) wind speed increments, respectively. As the wind speed increases by a factor of 1.3 U (30 percent), the rotor power increases to around 11.75 MW warranting its reduction to a factor of 0.43 approximately as shown by green dotted line. To achieve this, the blade is feathered by around 12 degrees for traditional control. This is also achieved by approximately feathering SePCaT30 by 26 degrees. If wind speed increases by a factor of 1.4 U (40 percent), the rotor power increases to around 14.30 MW warranting its reduction to a factor of 0.35 approximately as shown by light blue dotted line. To achieve this, the blade is pitched to feather by around 14 degrees for traditional control. This is also achieved by approximately feathering SePCaT30 by 32 degrees. The results, comparisons, and deductions are Proprietary to the wind turbine setup depicted in this paper. The wind velocity and power abatement factors and curve are obtained from model 5 MW wind turbine NREL [19]. One of the goals of these studies is to explore innovative blade designs as a result of deployment of SePCaT on the modified blade which is covered in Section 5.

5. Innovative Design Exploration

The goal of the new innovative design is to make a larger portion of the blade available for aerodynamic effectiveness. The root of the traditional blade is much thicker to withstand high stresses arising from blade loads. These stresses are more pronounced during high speeds (region 3) during which the entire blade is actively pitched to limit power so that they operate within the safe material stress limits of the wind turbine blade. In current wind turbine blades, part of the midspan of the blade and the tip contributes majority of the aerodynamic effectiveness needed by the rotor for power extraction. Figure 12 depicts the approximate allocated regions of blade aerodynamic (AR) and structural regions (ST) for the traditional blade and the traditional blade with SePCaT. BS stands for the main blade and S stands for SePCaT. Deployment of SePCaT allows the active pitching of predefined lengths of the tip of the blade (S) leading load abatement at high speeds instead of pitching the entire high inertia blade. SePCaT not only facilitates this highly efficient process but also leads to innovative blade design as depicted in Figure 13. The innovative blade design comprises two inner blades (B1, B2) arranged in parallel while maintaining the same SePCaT length. The goal of the new design for blades B1 and B2 is such that the entire blade along with the root is aerodynamically more effective when compared to the traditional design and contributes to the aerodynamic effectiveness for power extraction. This is due to thinner airfoil configurations near the root, while maintaining the blade stiffness for a larger length of the blade as a combination

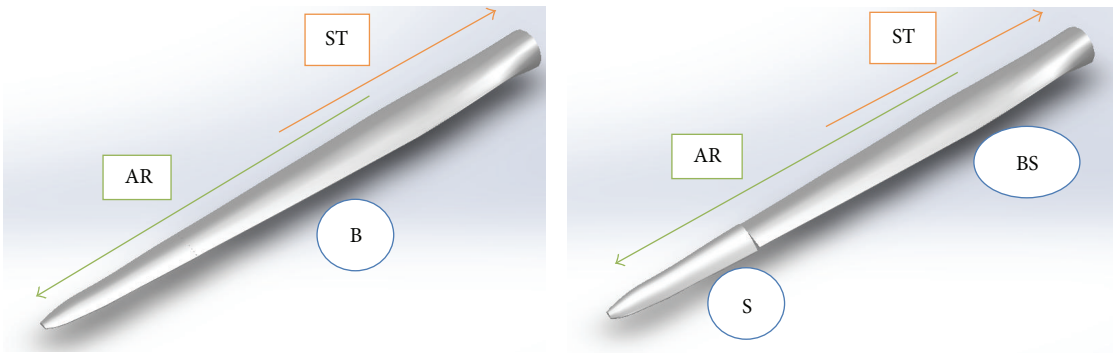

FIGURE 12: Approximate allocated regions of blade aerodynamic (AR) and structural regions (ST) for the traditional blade and the traditional blade with SePCaT. BS stands for the main blade and S stands for SePCaT.

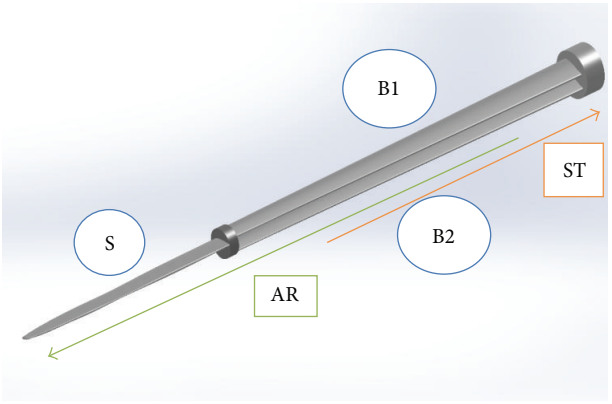

FIGURE 13: Approximate allocated regions of blade aerodynamic (AR) and structural regions (ST) modified design.

of two parallel stiffness elements to withstand high stresses. Iterative CFD analysis is conducted on the new design to optimize the lateral and linear sizes and length of inner blades B1 and B2; gap between B1 and B2; pitch angles for B1, B2, and SePCaT; and control angle for SePcaT are optimized for desired aerodynamic effectiveness. It is observed that lateral sizes of the inner blades B1 and B2 at 50 percent of blade BS and lengths of B1 and B2 at 80 percent of BS have similar aerodynamic effectiveness when compared to BS. It is also observed that 1.5 m gap between B1 and B2; B1 at an angle of 24 degrees; B2 at an angle of 25 degrees; and S at an angle of 25 degrees have the optimum aerodynamic effect.

Pneumatically actuated muscles (PAM) are envisioned to actuate the SePCaT by actively pitching the blade to either feather or stall. The goal of the actuator design is to keep them as light as possible while exhibiting strong actuator force. PAM have a high specific work and a good contraction ratio. An axially mounted 40 mm diameter, 1,250 mm long AM-AM PAM is selected with a mass of 1.25 kg. SePCaT-pitch angle is controlled using nonlinear sliding mode controllers (SMC) and its performance is compared to proportional-integral-derivative (PID) controllers. Sliding mode control is based on the control philosophy that a system is converged (made to reach) to a desired trajectory or the sliding monifold and controlled to stay on the sliding surface. Chapter 6 starting on page 83 of the author's Ph.D. dissertation [25] provides greater details on PAM and controller implementation and design. Readers are encouraged to refer to [25] for detailed reading on PAM and SMC Control Implementation.

6. Conclusions

This paper focused on the deployment and evaluation of a separated pitch control at blade tip (SePCaT) control strategy for large megawatt (MW) wind turbine blade and explorations of innovative blade designs as a result of such deployment. SePCaT results were compared to traditional blade by varying the full length blade angle. Comparisons of SePCaTs and traditional control with respect to power shedding capabilities in region 3 of the wind turbine are conducted at low, moderate, high, and extreme wind speed increments and variations. For low, moderate, high, and extreme wind speed variations treated as 10, 20, 30, and 40 percent of reference wind speeds, shedding of excessive rotor power is realized by feathering full length blade by 6, 9, 12, and 14 degrees, respectively, to maintain rated power. Feathering SePCaT30 by 14, SePCaT25 by 16, SePCaT20 by 26, or SePCaT15 by 30 degrees produces the same results at low wind speed increment and variation. Moderate wind speed increment is addressed by feathering SePCaT30 by 18, SePCaT25 by 26, or SePCaT20 by 30 degrees. SePCaT30 on the other hand can address high and extreme wind speed increments and variations by feathering to 26 and 30 degrees, respectively. The goal of the new design for blades B1 and B2 is such that the entire blade along with the root is aerodynamically more effective when compared to the traditional design and contributes to the aerodynamic effectiveness for power extraction. The authors plan to conduct aerodynamic and structural investigations using an iterative aerostructural design with the vision of optimizing mainstream blade aerodynamic and structural properties. The results, comparisons, and deductions are proprietary to the wind turbine setup depicted in this paper. The community is encouraged to conduct comprehensive analysis and testing before full functional deployment. Overall, the paper is expected to assist the community by giving them

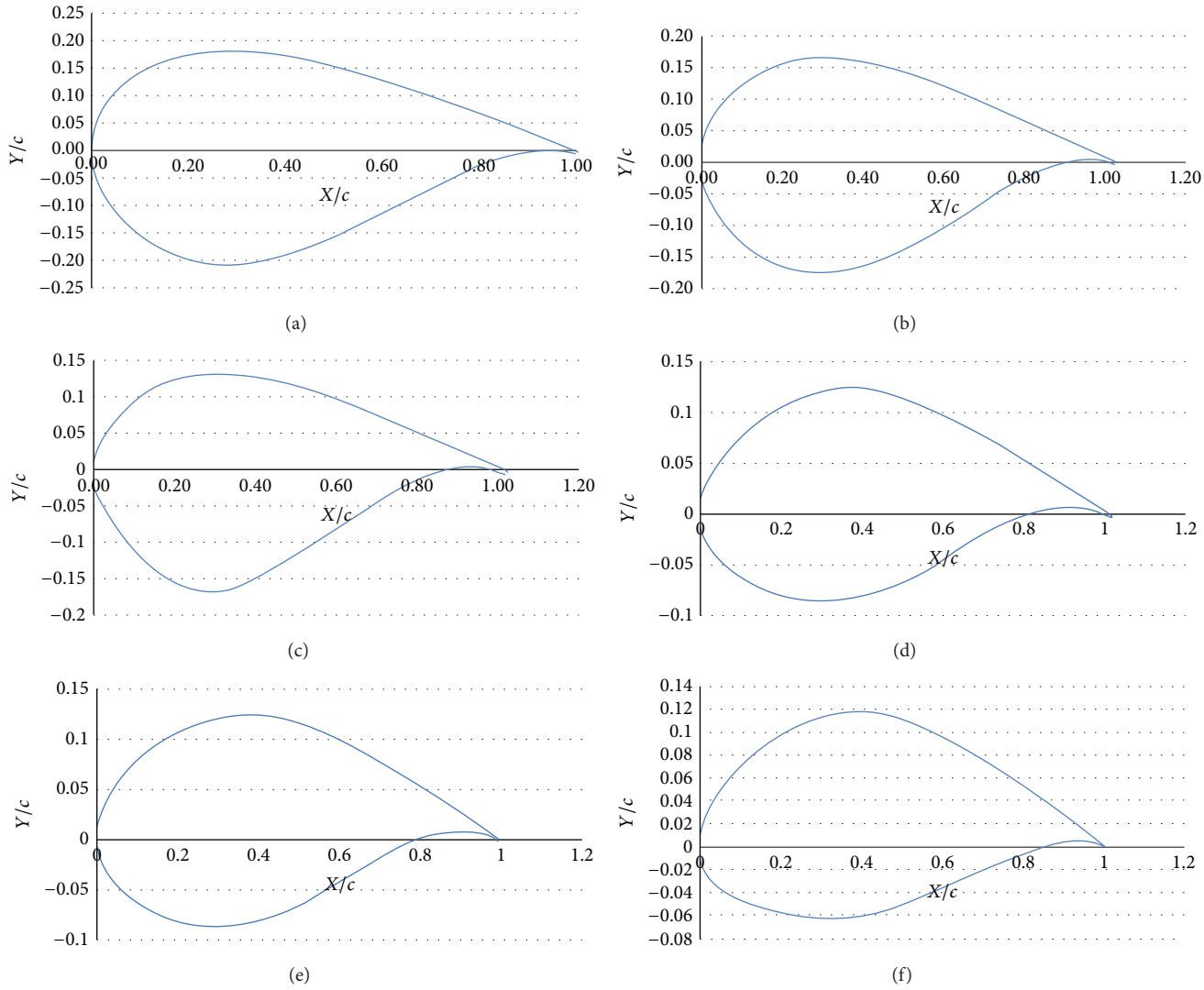

Figure 14: (a) DU40 airfoil, (b) DU35 airfoil, (c) DU30 airfoil, (d) DU25 airfoil, (e) DU21 airfoil, and (f) NACA 64 airfoil.

additional technology options and strategies in this ever important and evolving sector of renewable energy.

Appendix

Traditional Wind Turbine Specifications

This turbine stems from U.S. Department of Energy (DOE) National Renewable Energy Laboratory (NREL) conceptual studies conducted by the National Wind Technology Center (NWTC). This model turbine is being used by researchers throughout the world. This turbine has three blades and is an upwind variable-speed wind turbine. This model turbine has been inspired from published work of key turbine manufacturers and from models of Wind Partnerships for Advanced Component Technology project (WindPACT), Dutch Offshore Wind Energy Converter project (DOWEC), and recommendations for Design of Offshore Wind Turbines project (RECOFF). Jonkman et al. [19] have documented aerodynamics, structural, and control system properties as depicted in Table 3. Geometrical properties and coordinates for the construction of the 3D wind turbine blade are motivated by the model NREL offshore turbine.

The 3D turbine blade was constructed as shown in Figure 14 and Table 4 and as obtained from the NREL report [19]. The various airfoil shapes at different locations of the wind turbine blade are shown in Figures 14(a) through 14(f). The wind turbine blade is modeled in 3D by adopting SolidWorks CAD modeling software by Dassault systems.

Airfoil curves at various cross sections are generated using Cartesian coordinate systems. Airfoils at each section are scaled and rotated by their chord lengths and values of angular twists. Various cross sections are lofted and connected together using inbuilt CAD modeling interpolation routines. Blade roots start at a dimension of 2.8667 meters as some portion of the blade length is embedded within the rotor hub. Table 4 depicts the configuration. Here DFBR stands for distance from blade root. GT stands for

Table 3: Representative turbine specifications [19].

Rating	5 MW
Rotor orientation, configuration	Upwind, 3 blades
Control	Variable speed, collective pitch
Drive train	High speed, multiple-stage gearbox
Rotor, hub diameter	126 m, 3 m
Hub height	90 m
Cut-in, rated, cutout wind speed	3 m/s, 11.4 m/s, 25 m/s
Cut-in, rated rotor speed	6.9 rpm, 12.1 rpm
Rated tip speed	80 m/s
Rotor mass	110,000 kg
Nacelle mass	240,000 kg
Tower mass	347,460 kg
Coordinate location of CM	(−0.2 m, 0.0 m, 64.0 m)

Table 4: Sections of the wind turbine blade [19].

DFBR (m)	GT (°)	Chord (m)	Airfoil type
2.8667	13.308	3.542	Cylinder
5.6000	13.308	3.854	Cylinder
8.3333	13.308	4.167	Cylinder
11.7500	13.308	4.557	DU40
15.8500	11.480	4.652	DU35
19.9500	10.162	4.458	DU35
24.0500	9.011	4.249	DU30
28.1500	7.795	4.007	DU25
32.2500	6.544	3.748	DU25
36.3500	5.361	3.502	DU21
40.4500	4.188	3.256	DU21
44.5500	3.125	3.010	NACA64
48.6500	2.310	2.764	NACA64
52.7500	1.526	2.518	NACA64
56.1667	0.863	2.313	NACA64
58.9000	0.370	2.086	NACA64
61.6333	0.106	1.419	NACA64

geometrical twist angles of the blades airfoils at various blade stations. DU and NACA are standard airfoils.

Conflict of Interests

The authors declare that there is no conflict of interests with regard to the publication of this paper. The authors declare that this paper has not been influenced by financial gain.

References

[1] M. Imraan, R. N. Sharma, and R. G. J. Flay, "Wind tunnel testing of a wind turbine with telescopic blades: the influence of blade extension," *Energy*, vol. 53, pp. 22–32, 2013.

[2] R. Agarwala and P. I. Ro, "3D analysis of lift and moment adaptation via control surface deployments on a 5 MW wind turbine blade," *Wind Engineering*, vol. 37, no. 5, pp. 447–468, 2013.

[3] G. Peter, F. M. Silkeborg, and S. C. B. Hojbjer, "Pitch system balancing for wind turbine," European Patent, EP2455611A2, 2012.

[4] S. Daynes and P. M. Weaver, "Design and testing of a deformable wind turbine blade control surface," *Smart Materials and Structures*, vol. 21, Article ID 105019, pp. 1–10, 2012.

[5] T. K. Barlas, G. J. van der Veen, and G. A. M. van Kuik, "Model predictive control for wind turbines with distributed active flaps: incorporating inflow signals and actuator constraints," *Wind Energy*, vol. 15, no. 5, pp. 757–771, 2012.

[6] T. K. Barlas and G. A. M. van Kuik, "Review of state of the art in smart rotor control research for wind turbines," *Progress in Aerospace Sciences*, vol. 46, no. 1, pp. 1–27, 2010.

[7] Y. L. Bai, X. Y. Ma, and X. Ming, "Lift enhancement of airfoil and tip flow control for wind turbine," *Applied Mathematics and Mechanics*, vol. 32, no. 7, pp. 825–836, 2011.

[8] T. Lee and Y. Y. Su, "Lift enhancement and flow structure of airfoil with joint trailing-edge flap and Gurney flap," *Experiments in Fluids*, vol. 50, no. 6, pp. 1671–1684, 2011.

[9] S. Daynes and P. M. Weaver, "A morphing trailing edge device for a wind turbine," *Journal of Intelligent Material Systems and Structures*, vol. 23, no. 6, pp. 691–701, 2012.

[10] X. Lachenal, S. Daynes, and P. M. Weaver, "Review of morphing concepts and materials for wind turbine blade applications," *Wind Energy*, vol. 16, no. 2, pp. 283–307, 2013.

[11] I. Houtzager, J.-W. van Wingerden, and M. Verhaegen, "Rejection of periodic wind disturbances on a smart rotor test section using lifted repetitive control," *IEEE Transactions on Control Systems Technology*, vol. 21, no. 2, pp. 347–359, 2013.

[12] P. Versailles, S. Ghosh, H. Duc, and C. Masson, "Preliminary assessment of wind turbine blade lift control via plasma actuation," *Wind Engineering*, vol. 35, no. 3, pp. 339–356, 2011.

[13] J. R. Bottalla, M. B. Bragg, J. J. Sheahan Jr., and C. M. Winkler, "Performance of an airfoil with a power-saving, tab-assisted flap system," in *Proceedings of the 29th AIAA Applied Aerodynamics Conference*, June 2011.

[14] J. Heinz, N. N. Sørensen, and F. Zahle, "Investigation of the load reduction potential of two trailing edge flap controls using CFD," *Wind Energy*, vol. 14, no. 3, pp. 449–462, 2011.

[15] H. Markou, P. B. Andersen, and G. C. Larsen, "Potential load reductions on megawatt turbines exposed to wakes using individual-pitch wake compensator and trailing-edge flaps," *Wind Energy*, vol. 14, no. 7, pp. 841–857, 2011.

[16] P. B. Andersen, L. Henriksen, M. Gaunaa, C. Bak, and T. Buhl, "Deformable trailing edge flaps for modern megawatt wind turbine controllers using strain gauge sensors," *Wind Energy*, vol. 13, no. 2-3, pp. 193–206, 2010.

[17] S. J. Johnson, J. P. Baker, C. P. van Dam, and D. Berg, "An overview of active load control techniques for wind turbines with an emphasis on microtabs," *Wind Energy*, vol. 13, no. 2-3, pp. 239–253, 2010.

[18] D. G. Wilson, D. E. Berg, M. F. Barone, J. C. Berg, B. R. Resor, and D. W. Lobitz, "Active aerodynamic blade control design for load reduction on large wind turbines," in *Proceedings of the European Wind Energy Conference & Exhibition (EWEC '09)*, pp. 643–678, March 2009.

[19] J. Jonkman, S. Butterfield, W. Musial, and G. Scott, "Definition of a 5-MW reference wind turbine for offshore system development," Technical Report-NREL/TP-500-38060, Task No. WER5.3301, 2009.

[20] C. P. van Dam, R. Chow, J. R. Zayas, and D. E. Berg, "Computational investigations of small deploying tabs and flaps for aerodynamic load control," *Journal of Physics: Conference Series*, vol. 75, Article ID 012027, pp. 1–10, 2007.

[21] A. M. Georggescu, S. C. Georggescu, S. Bernard, and C. L. Cosoiu, "Comsol multiphysics versus fluent: 2d numerical simulation of the stationary flow around a blade of the achard turbine," in *Proceedings of the 3rd Workshop on Vortex Dominated Flows*, vol. 52, pp. 13–21, 2007.

[22] F. Zhang and D. Söffker, "Active flutter suppression of a nonlinear aeroelastic system using PI-observer," in *Proceedings of the 9th International Conference on Motion and Vibration Control (MOVIC '08)*, pp. 367–376, September 2008.

[23] T. O'Neil and T. W. Strganac, "Aeroelastic response of a rigid wing supported by nonlinear springs," *Journal of Aircraft*, vol. 35, no. 4, pp. 616–622, 1998.

[24] Y. C. Fung, *An Introduction to the Theory of Aeroelasticity*, Wiley, 1955.

[25] R. Agarwala, *Separated pitch control at tip (SePCaT): a novel blade design and associated control strategies for large MW wind turbines [Ph.D. dissertation]*, 2014, http://repository.lib.ncsu.edu/ir/handle/1840.16/9829.